Revista Brasileira de Cartografia
ISSN 1808-0936 | https://doi.org/10.14393/revbrascartogr
Sociedade Brasileira de Cartografia, Geodésia, Fotogrametria e Sensoriamento Remoto

Performance of Ion-Free and GRAPHIC Combinations in Multi-GNSS PPP under Different Ionospheric Conditions in Brazil

Desempenho de Combinações Ion-Free e GRAPHIC no PPP Multi-GNSS sob Diferentes Condições Ionosféricas no Brasil

João Pedro Voltare Zaupa [1], Daniele Barroca Marra Alves [2] and Paulo de Tarso Setti Junior [3]

1 São Paulo State University (UNESP), Graduate Program in Cartographic Sciences (PPGCC), Presidente Prudente, Brazil. jp.zaupa@unesp.br.
ORCID: https://orcid.org/0000-0002-1123-7578.
2 São Paulo State University (UNESP), Department of Cartography, Presidente Prudente, Brazil. daniele.barroca@unesp.br.
ORCID: https://orcid.org/0000-0002-9033-8499.
3 São Paulo State University (UNESP), Department of Cartography, Presidente Prudente, Brazil. p.setti@unesp.br.
ORCID: https://orcid.org/0000-0001-5080-1832.

Recebido: 02.2026 | Aceito: 07.2026

Abstract: This paper preliminarily evaluates the performance of multi-GNSS Precise Point Positioning (PPP) using the GRAPHIC method and dual- (IF2) and triple-frequency (IF3) ion-free combinations under contrasting ionospheric conditions in Brazil. RINEX3 data from five stations of the Brazilian Network for Continuous Monitoring of GNSS Systems (RBMC) were processed for March and June 2024, totaling 60 days of observations, with daily three-hour sessions starting at 00:00 UTC. The assessment considered satellite availability, solution geometry through position dilution of precision (PDOP), convergence time, positioning discrepancies in the Local Geodetic System, and pseudorange and carrier-phase residuals as a function of elevation angle. The results show that IF2 achieved the best overall performance, preserving greater multi-constellation availability, with approximately 28 satellites per epoch and PDOP close to 1, while also providing faster convergence and smaller final discrepancies, especially in June. GRAPHIC showed greater dispersion, associated with the propagation of pseudorange noise into the quasi-carrier observable. IF3, in turn, was penalized by the lower effective availability of simultaneous triple-frequency observations, decreasing to approximately 12 satellites per epoch and increasing PDOP, which resulted in longer convergence times and larger residual errors, especially in the vertical component. The results indicate that the direct application of triple-frequency combinations, under the tracking conditions of the analyzed stations, did not provide systematic improvement over IF2. Therefore, its operational adoption requires adequate multifrequency availability, quality control, and explicit modeling of inter-frequency biases.
Keywords: PPP. Multi-GNSS. Ion-free combination. GRAPHIC. Ionosphere.

Resumo: Este artigo avalia, de forma preliminar, o desempenho do Posicionamento por Ponto Preciso (PPP) multi-GNSS com os métodos *Group and Phase Ionospheric Calibration* (GRAPHIC) e combinações *ion-free* de dupla (IF2) e tripla frequência (IF3), considerando condições ionosféricas contrastantes no Brasil. Foram processados dados RINEX3 de cinco estações da Rede Brasileira de Monitoramento Contínuo dos Sistemas GNSS (RBMC) para março e junho de 2024, totalizando 60 dias de observações, com sessões diárias de três horas iniciadas às 0h UTC. A avaliação considerou a disponibilidade de satélites, a geometria da solução por meio da diluição de precisão posicional (*position dilution of precision* - PDOP), o tempo de convergência, as discrepâncias posicionais no Sistema Geodésico Local e os resíduos de pseudodistância e fase em função do ângulo de elevação. Os resultados mostram que a IF2 manteve o melhor desempenho geral, preservando maior disponibilidade multi-constelação, com cerca de 28 satélites por época e PDOP próximo de 1, além de apresentar convergência mais rápida e menores discrepâncias finais, especialmente em junho. O GRAPHIC apresentou maior dispersão, associada à propagação do ruído da pseudodistância na observável *quasi-carrier*. A IF3, por sua vez, foi penalizada pela menor disponibilidade efetiva de observações simultâneas em três frequências, com redução para aproximadamente 12 satélites por época e aumento do PDOP, resultando em maior tempo de convergência e erros residuais mais elevados, sobretudo na componente vertical. Os resultados indicam que a aplicação direta da tripla frequência, nas condições de rastreio das estações analisadas, não garantiu melhoria sistemática em relação à IF2. Assim, sua adoção operacional requer disponibilidade multifrequência adequada, controle de qualidade e modelagem explícita de vieses interfrequência.
Palavras-chave: PPP. Multi-GNSS. Combinação livre da ionosfera. GRAPHIC. Ionosfera.

1 INTRODUCTION

The continuous modernization of Global Navigation Satellite System (GNSS) constellations has expanded the scope of high-precision positioning techniques, including Precise Point Positioning (PPP). In this method, centimeter-level geodetic positioning can be achieved using a single receiver, provided that pseudorange and carrier-phase observations are processed together with precise orbit and clock products, as well as appropriate atmospheric models and corrections (Ge et al., 2019; Elsheikh et al., 2023). This scenario has been particularly favored by the consolidation of global services that routinely estimate precise products and by the increasing adoption of multi-GNSS solutions in scientific and engineering applications (Elsheikh et al., 2023). In this context, the International GNSS Service (IGS) Multi-GNSS Experiment (MGEX) stands out for generating and providing precise multi-GNSS products, including orbits (SP3), clocks (CLK), and associated biases, such as Observable Specific Biases (OSBs), thereby enabling the consistent integration of different constellations in PPP processing (Montenbruck et al., 2017).

Historically, PPP has been widely adopted mainly through the dual-frequency ion-free linear combination, as it provides a direct way to eliminate the first-order ionospheric term, one of the main error sources in GNSS observations (Tegedor & Øvstedal, 2014). This approach remains a standard in operational applications, partly because of its consistency with the products commonly used in processing, which helps explain why traditional services are still mostly based on two carrier frequencies. However, the availability of additional signals in modern constellations, such as L5 for GPS, E5a/E5b and E6 for Galileo, B2a/B2b for BeiDou, and L3 for GLONASS-K, has enabled the use of triple-frequency ion-free combinations (Su & Jin, 2019; Wang et al., 2022). In principle, this expansion allows combinations with different stochastic properties and greater tolerance to adverse observational conditions. Nevertheless, such combinations may also introduce stronger noise amplification and changes in ambiguity behavior, which do not always result in effective performance improvements when compared with the traditional dual-frequency model (Su et al., 2020; Tian et al., 2026). In parallel, alternative strategies such as the Group and Phase Ionospheric Calibration (GRAPHIC) method have been employed especially for single-frequency receivers. This method enables the mitigation of the first-order ionospheric effect by combining pseudorange and carrier-phase observations, although at the cost of increased observation noise (Choy, 2009; Shi et al., 2012). The literature also shows that PPP performance is sensitive to ionospheric conditions, especially at low latitudes, where the variability of the Total Electron Content (TEC) can become more intense and dynamically complex (Su et al., 2020; Elsheikh et al., 2023; Glaner & Weber, 2023). During periods of high ionospheric activity, associated, for example, with geomagnetic storms, scintillation, and irregularities such as ionospheric plasma bubbles, fluctuations in the propagation medium degrade observation quality, increase residuals, and may prolong the convergence period of the solution (Moraes et al., 2014; Veettil et al., 2020).

Although recent studies have reported benefits associated with the use of multifrequency observations in PPP, such as reduced convergence time, increased observational redundancy, and improved support for ambiguity estimation, these gains depend on the effective availability of signals, the consistency of the precise products used, the modeling of inter-frequency biases, and the local ionospheric conditions. Studies such as those by Deo and El-Mowafy (2017) and Su et al. (2020) demonstrate performance improvements with the use of multiple frequencies, while more recent investigations highlight the importance of inter-frequency bias modeling and multifrequency integration in multi-GNSS PPP solutions (Wang et al., 2022; Wu et al., 2022; Yang et al., 2024). However, the operational application of these strategies may be limited by receiver heterogeneity, incomplete support for specific signals, and firmware or tracking-channel restrictions, as observed for BeiDou-3 in international multi-GNSS networks (Zajdel et al., 2022). Furthermore, in low-latitude regions such as Brazil, the Equatorial Ionization Anomaly and ionospheric scintillation introduce significant spatial and temporal irregularities in the TEC, which can degrade the quality of the observables, reduce tracking continuity, and compromise the simultaneous availability of multiple frequencies. Recent studies have also shown the impact of scintillation on GNSS availability and precise positioning in equatorial regions, reinforcing the need for specific assessments under these conditions (Aguiar et al., 2025; Marques et al., 2025).

Therefore, this paper aims to evaluate the performance of dual- and triple-frequency ion-free linear combinations, as well as the GRAPHIC method, in multi-GNSS PPP by integrating GPS, GLONASS, Galileo, and BeiDou observations under low and high ionospheric variability conditions. For this purpose, data collected by Brazilian stations located in a low-latitude region are analyzed, considering distinct periods of ionospheric activity. The evaluation metrics include: (1) positioning accuracy, considering the discrepancy vector and the propagation of the covariance matrix of the adjusted positional parameters; (2) observation residuals, assessed separately for pseudorange and carrier-phase measurements; and (3) convergence time, defined as the interval required to reach predefined horizontal (H) and vertical (V) accuracy thresholds. Furthermore, this paper is an extended version of the work presented by Zaupa et al. (2025) at the I CIRF & VIII SIMGEO – *Regularização Fundiária Plena & Geotecnologias*.

In addition to this introduction, the paper is organized as follows. Section 2 presents the theoretical background of the GRAPHIC and ion-free combinations and their application in PPP. Section 3 describes the materials and methods, including the data, processing strategies, and evaluation criteria. Section 4 discusses the results, comparing the performance of the combinations under different ionospheric conditions. Finally, Section 5 presents the conclusions, summarizing the main findings and their implications for high-precision GNSS positioning.

2 ION-FREE LINEAR COMBINATION

The propagation of GNSS signals through the Earth's atmosphere is strongly affected by the ionosphere, especially in regions close to the magnetic equator, where intense spatial and temporal gradients in electron density are commonly observed. As a dispersive medium, the ionosphere affects the group and phase propagation of GNSS signals in different ways. The interaction with free electrons reduces the group velocity, causing a delay in pseudorange observations, while the phase velocity becomes greater than the speed of light in vacuum, resulting in an advance in carrier-phase observations. Both effects depend on the signal frequency and the TEC along the satellite–receiver line of sight (Jiang et al., 2024). Most of this effect is associated with the F region, particularly the F2 layer, whose peak electron density typically occurs between 250 and 400 km in altitude and may reach values on the order of 10^5 to 10^6 electrons per cubic centimeter (Hobiger & Jakowski, 2017; Sousasantos et al., 2024). TEC variations are related to factors such as latitude, local time, season, and solar and geomagnetic activity, and may lead to severe effects such as scintillation, ionospheric plasma bubbles, and cycle slips (Matsuoka et al., 2013; Veettil et al., 2020; Zaupa et al., 2022; Dal Poz et al., 2025; Yang & Morton, 2025; Zaupa et al., 2026b). Different strategies can be employed to mitigate ionospheric effects in GNSS observations. Among them, the GRAPHIC method, presented in Section 2.1, is based on the combination of pseudorange and carrier-phase observations, whereas ion-free linear combinations exploit the dependence of the ionospheric delay on the inverse square of the signal frequency. This technique is based on the combination of two or more observations collected simultaneously on different frequencies. Sections 2.2 and 2.3 present the dual- and triple-frequency ion-free combinations, respectively. Section 2.4 discusses the noise amplification caused by this linear combination.

2.1 GRAPHIC method

The GRAPHIC method is an ionospheric mitigation strategy mainly intended for applications using single-frequency receivers and is based on the concept of a "*quasi-carrier*" observable (Choy, 2009). In this method, pseudorange observations are used as provided in RINEX files and may be previously corrected by ionospheric models, such as the Klobuchar model (1987). The main characteristic of the method lies in the combination of pseudorange (P) and carrier-phase (L) observations, taking advantage of the fact that first-order ionospheric effects act with the same magnitude on both observables, but with opposite signs. Thus, by combining these quantities, this effect can be directly eliminated. Considering all observations expressed in meters, the resulting observable, called *quasi-carrier* ($\overline{\varphi}$), can be expressed as (Choy, 2009):

$$\overline{\varphi} = \frac{P + L}{2}. \tag{1}$$

Therefore, the combination results in an increase in the effective noise of the observation, which may

 DOI: http://dx.doi.org/10.14393/rbcv78n0a-81258

negatively affect the precision of the solution, especially in high-accuracy applications. Despite this limitation, the method presents relevant advantages in scenarios with limited frequency availability, representing a viable alternative for applications based on low-cost receivers.

2.2 Dual-frequency linear combination (IF2)

Ion-free combinations can be applied to both pseudorange and carrier-phase observations. For signals 1 and 2 with frequencies $f1$ and $f2$, respectively, the multiplying coefficients m_1 and $m_2$are defined as (Hauschild, 2017):

$$m_1 = \frac{f1^2}{f1^2 - f2^2}, m_2 = \frac{f2^2}{f1^2 - f2^2} \tag{2}$$

resulting in the following expressions for the pseudorange (P_{if}) and carrier-phase (L_{if}) combinations:

$$\begin{aligned} P_{if} &= m_1 P1 - m_2 P2, \\ L_{if} &= m_1 L1 - m_2 L2, \end{aligned} \tag{3}$$

where $P1$ and $L1$, $P2$ and $L2$ are the pseudorange and carrier-phase observations for signals 1 and 2, respectively. The use of these combinations is widely adopted in PPP, mainly due to their simple implementation and their effective elimination of first-order ionospheric delays. In general, combinations involving more widely separated frequencies, such as GPS L1 and L5, produce lower combined noise. Conversely, combinations between close frequencies, such as Galileo E5a/E5b, result in high noise amplification, which may limit their practical use (Schönemann, 2014).

2.3 Triple-frequency linear combination (IF3)

This section presents a PPP model based on a triple-frequency ion-free linear combination, formulated to reduce noise propagation while preserving the geometry, with the aim of favoring faster ambiguity convergence when compared with the traditional dual-frequency model (Deo & El-Mowafy, 2017). The linear combination is consistently applied to both carrier-phase and pseudorange observations. The geometry-preserving condition is defined by the sum of the combination coefficients being equal to 1, while the condition for eliminating the first-order ionospheric effect is represented by a relationship between these coefficients and the frequency multipliers associated with each constellation (Table 1).

Table 1 – Fundamental frequency multipliers (10.23 MHz) of the GNSS constellations.

System	**Signals and Fundamental Frequency Multipliers**		
GPS	L1: 154	L2: 120	L5: 115
GLONASS-K2	G1: 156.5	G2: 122	G3: 117.5
Galileo	E1: 154	E5a: 115	E5b: 118
BeiDou	B1: 152.6	B3: 124	B2: 118

Source: Adapted from Teunissen and Montenbruck (2017).

Noise propagation is minimized by minimizing a noise amplification factor derived from the three frequencies. Considering three phase or code signals observed at frequencies $f1$, $f2$ and $f3$, the linear combination can be expressed as (Deo & El-Mowafy, 2017; Su et al., 2020):

$$\begin{aligned} P_{if} &= \alpha P1 + \beta P2 + \gamma P3, \\ L_{if} &= \alpha L1 + \beta L2 + \gamma L3, \end{aligned} \tag{4}$$

where α, β and γ are the coefficients of the linear combination. Three conditions are imposed to construct an optimized combination:

1. Geometry preservation: the sum of the coefficients must be equal to 1: $\alpha + \beta + \gamma = 1$;

2. Elimination of the first-order ionospheric effect: based on the inverse-square dependence on frequency: $\alpha f1^{-2} + \beta f2^{-2} + \gamma f3^{-2} = 0$;
3. Minimum noise propagation: assuming equivalent noise in the three observations, the noise amplification factor ε is defined as: $\varepsilon = \alpha^2 + \beta^2 + \gamma^2$.

By minimizing ε, a more stable combination suitable for ambiguity estimation is obtained, contributing to a reduction in PPP convergence time. The coefficients can be obtained through sequential substitution in the equations described above, resulting in a quadratic equation of the form:

$$A\gamma^2 + B\gamma + C = 0, \quad (5)$$

where the coefficients A, B and C depend on the frequency multipliers given in Table 1.

2.4 Noise Amplification in the Linear Combination

Although ion-free combinations are effective in eliminating the first-order ionospheric term, they inevitably amplify the noise in the resulting observations due to the weights assigned to the different frequencies. This amplification can be represented by a characteristic factor for each set of frequencies used and is directly related to the relative separation between them. It is important to emphasize that this increase is not limited to the simple propagation of the covariance of the original observations: it also includes the contribution of multipath, which manifests differently at each frequency and, when combined, may further intensify the effective noise in ion-free observations. Figure 1 presents the values of ε for different dual- and triple-frequency combinations of GNSS signals, considering the most commonly used signals in each system, organized as signals 1, 2, and 3, respectively. The following correspondence was adopted: L1, L2, and L5 for GPS; G1, G2, and G3 for GLONASS (CDMA); E1, E5a, and E5b for Galileo; and B1, B3I, and B2I for BeiDou. Each combination represents the pair or set of three signals used to form the ion-free observable, highlighting how frequency selection influences the level of associated noise amplification.

Figure 1 – Noise amplification in ion-free combinations (dual- and triple-frequency).

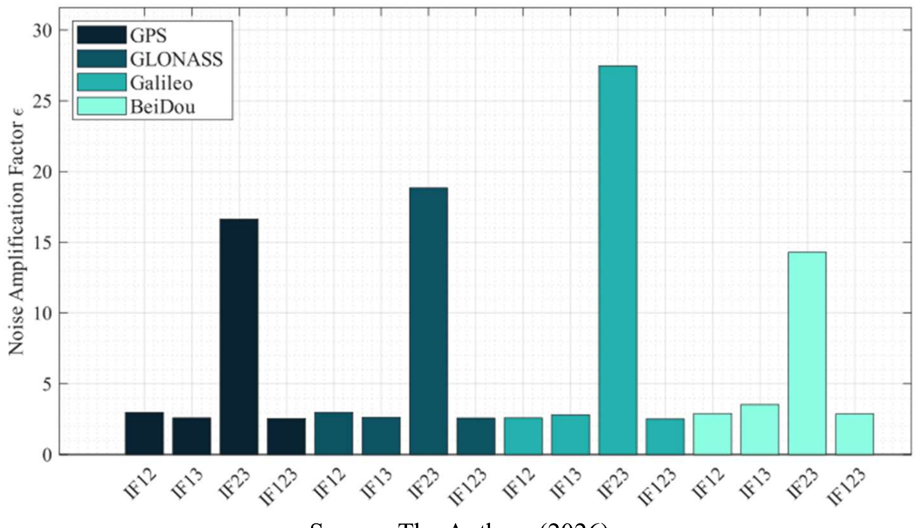

Source: The Authors (2026).

Combinations with close frequencies, such as GPS L2-L5 or Galileo E5a-E5b, tend to present significant amplification, which results in greater residual dispersion, lower reliability of the estimated ambiguities, and longer PPP convergence time (Schönemann, 2014; Tegedor & Øvstedal, 2014; Deo & El-Mowafy, 2017). Therefore, the choice of the most appropriate combination should consider the balance between the removal of the ionospheric effect and the penalty introduced by noise amplification.

3 METHODOLOGY

In this study, GNSS data from five stations of the Brazilian Network for Continuous Monitoring of

GNSS Systems (RBMC), distributed across the country, were used: BOAV, BRAZ, PERC, PPTE, and RSSL (Figure 2). For the analysis of ionospheric scintillation, data from stations belonging to the National Institute of Science and Technology – GNSS Technology to Support Air Navigation (INCT GNSS-NavAer) were employed: POAL, PRU2, STMC, STMN, and STNT (Monico et al., 2022). The data were obtained in RINEX3 format, with continuous records during two distinct 30-day periods: March and June 2024, totaling 60 days of observations. For each month, a three-hour interval was processed each day, starting at 00:00 UTC. These periods were selected to represent distinct ionospheric conditions: March as a typical equinoctial transition period and June as representative of winter in the Southern Hemisphere. The GNSS observations were processed using static multi-GNSS PPP approaches, applying the GRAPHIC, IF2, and IF3 combinations with the APPPOLO (Advanced Precise Point Positioning software for Optimized LOcalization) software (Zaupa, 2025; Zaupa et al., 2026a). Each configuration was independently applied to the 60-day dataset, while keeping the remaining modeling and adjustment parameters fixed, as described in Table 2.

Figure 2 – RBMC and INCT GNSS-NavAer stations selected for the experiment.

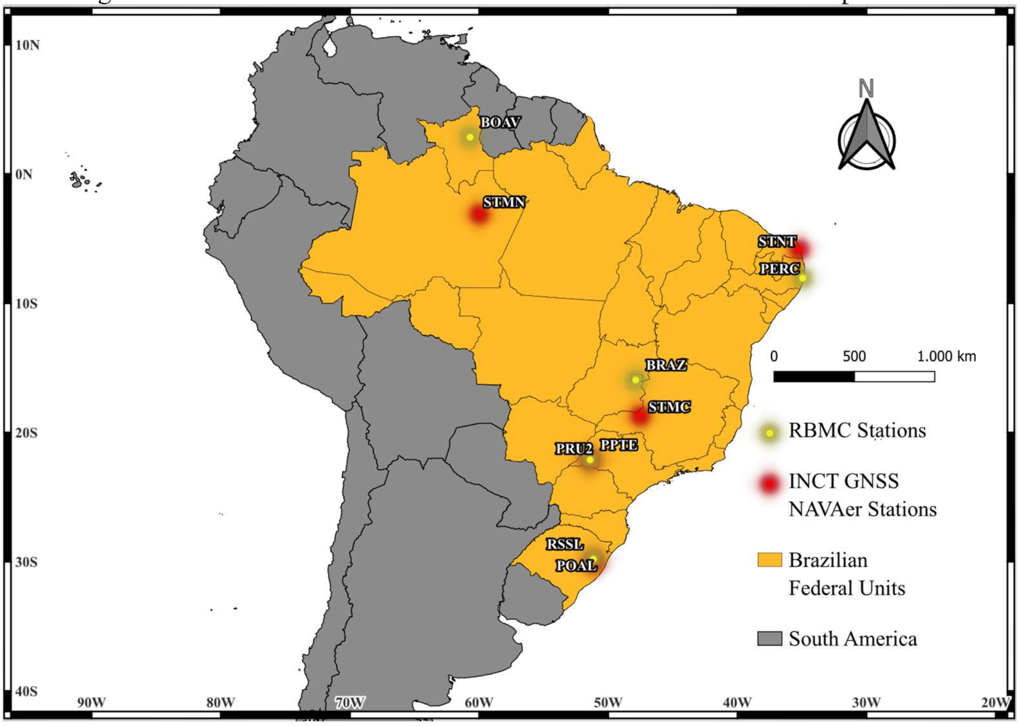

Source: The Authors (2026).

Table 2 – Strategies for PPP processing using the APPPOLO software.

Parameter	Strategy
Observables	GPS: L1 C/A, L2 P(Y), L5; GLONASS: G1, G2, G3; Galileo: E1, E5a, E5b; BeiDou: B1, B2I, B3I.
Uncertainties	σ_{P1}=0.8 m; $\sigma_{P2}=\sigma_{P3}$=1.0 m; σ_{L1}=0.008 m; $\sigma_{L2}=\sigma_{L3}$=0.010 m (weighted by the inverse of the sine of the elevation angle).
Estimator	Robust Adaptive Kalman Filtering (Zhang et al., 2021).
Masks	Elevation: 10°; SNR: 27 dBHz.
Orbits and clocks	Precise ephemerides (SP3) and clock files (CLK) from CODE, in the IGS20 reference frame, with temporal resolutions of 5 minutes and 30 seconds, respectively. Interpolated to the signal transmission time using Moving Window Lagrange Interpolation of degree 9 (Zaupa, 2025).
Neutrosphere effects	VMF3 mapping function (Landskron & Böhm, 2018), zenith wet delay (VMF3), zenith hydrostatic delay (VMF3), and estimated residual component.
Coordinates and ambiguities	Coordinates estimated as constants. Ambiguities estimated as white noise when cycle slips occur, detected using the TurboEdit algorithm (Blewitt, 1990).
Other systematic effects	Phase wind-up (Wu et al., 1993), Sagnac effect (Ashby, 2004), Phase Center Offset and Variation (PCO/PCV) (Montenbruck et al., 2015), Observable Specific Biases (OSBs) (Li & Yuan, 2021), solid Earth and ocean tides (Kouba et al., 2017), and relativistic effects on clock and range (Ashby, 2003).

Source: The Authors (2026).

 DOI: http://dx.doi.org/10.14393/rbcv78n0a-81258

3.1 Ionospheric Variability during the Processing Period

To illustrate the ionospheric behavior during the analyzed periods, Figure 3 presents the temporal evolution of the S4 index based on GNSS observations recorded at the INCT GNSS-NavAer stations for March and June 2024. This index is widely used as an indicator of ionospheric scintillation intensity and reflects rapid variations in GNSS signal amplitude (Veettil et al., 2020). The bars represent the hourly mean S4 values throughout each month, together with the number of observations for which S4 exceeded 0.7, considering the complete monthly datasets. A fluctuation pattern can be observed over time, with higher values associated with greater ionospheric instability in March, which may directly affect positioning accuracy and the convergence time of PPP solutions.

Figure 3 – S4 index for March (left) and June (right) 2024, considering the INCT GNSS-NavAer stations. The bar plot represents the hourly mean S4 throughout the month, as well as the count of epochs with S4 > 0.7, considering all monthly observations.

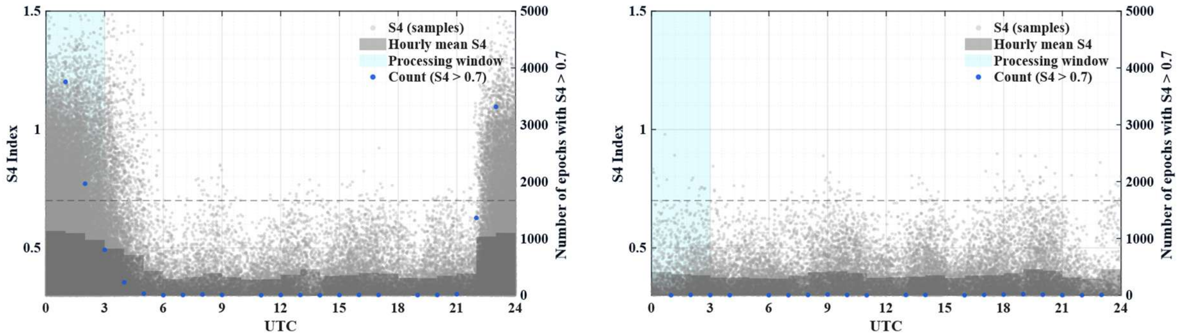

Source: The Authors (2026).

In June, the S4 index values remained predominantly below 0.6 throughout the day, with small fluctuations and no significant peaks. Considering only values above 0.3, the mean S4 was 0.39. During the observation window between 00:00 and 03:00 UTC, only 21 instances presented S4 values greater than 0.7. This behavior reflects relatively calm ionospheric conditions, which are favorable to the stability of high-precision GNSS solutions. In contrast, in March, a marked increase in S4 values was observed between 21:00 and 02:00 UTC, with peaks exceeding 1.0 at several moments. During the processing interval between 00:00 and 03:00 UTC, the mean S4 was 0.54, with a total of 11,300 occurrences above 0.7. This pattern is characteristic of strong amplitude scintillation and is consistent with the typical nighttime behavior of the ionosphere in the equatorial region, when irregularities such as plasma bubbles are more frequent (Basu et al., 2002).

3.2 Evaluation Metrics

The quality assessment of the multi-GNSS PPP solutions was conducted using three main metrics: positioning accuracy, observation residuals, and convergence time. Accuracy was obtained from the discrepancy between the estimated coordinates and a reference position, adopting the SIRGAS-CON coordinates, updated to the processing epoch. The analysis was performed in the Local Geodetic System (LGS), considering the propagation of the covariance matrix of the estimated positional parameters. To provide a broader representation of performance over the processing epochs, the three-dimensional component of the error and standard deviation was analyzed through the Root Mean Square Error (RMSE), thereby summarizing the accuracy effectively achieved at each processing epoch. The quality of the GNSS observation adjustment was evaluated using the Root Mean Square (RMS) of the residuals, which expresses the degree of compatibility between the observations and the adopted model. This indicator is sensitive to different degradation sources, including measurement noise, modeling imperfections, and atmospheric disturbances that are not properly compensated, directly reflecting the internal consistency of the adjustment (Monico, 2008).

The analysis of convergence time aimed to identify the epoch at which the solution reached a predefined accuracy level and remained stable until the end of the session. For this purpose, a threshold of 10 cm was adopted for both the horizontal and vertical components (Xiang et al., 2020). Convergence was considered to occur at the first epoch in which the positioning accuracy fell below these thresholds and continuously remained within this criterion.

4 RESULTS AND ANALYSES

Before discussing the accuracy indicators, Figure 4 presents the mean satellite availability and the geometry associated with the evaluated combinations for each station. The geometry is assessed using the Position Dilution of Precision (PDOP), an indicator that describes the geometric quality of the satellite set in the adjustment and quantifies the degree of measurement-error amplification in the position estimation.

Figure 4 – Mean geometry of the multi-GNSS PPP solution over the complete set of analyzed days: mean number of satellites, with contribution by constellation, and mean PDOP per station for (a) IF2 and GRAPHIC and (b) IF3.

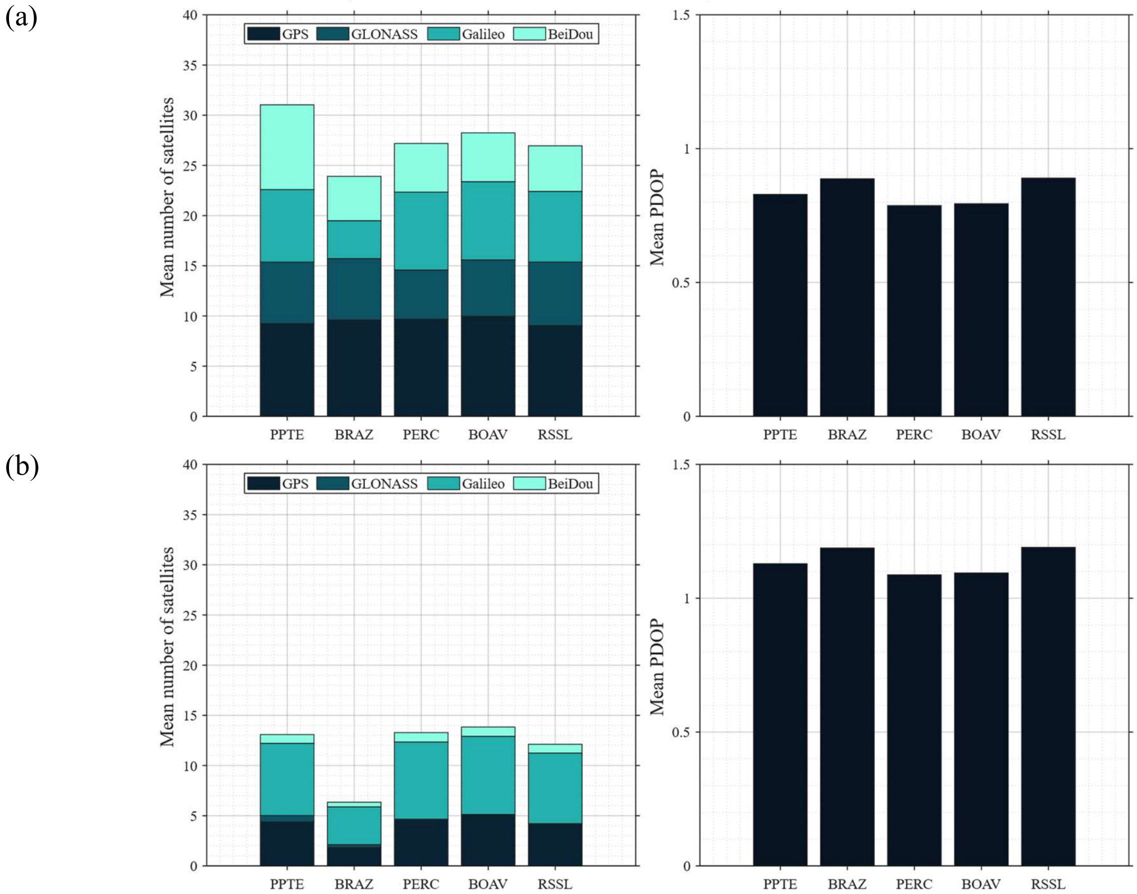

Source: The Authors (2026).

A significant difference between the strategies can be observed: the dual-frequency ion-free combination maintains a multi-constellation set with an average of 28 satellites per epoch, with the minimum occurring at BRAZ, with 24 satellites. On average, this set is distributed among GPS (10), GLONASS (6), Galileo (7), and BeiDou (5). In contrast, for the triple-frequency ion-free combination, availability decreases sharply to 12 satellites per epoch, with a critical reduction at BRAZ, where only 6 satellites are available, reflecting the lower availability of simultaneous triple-frequency observations. In addition, the constellation-wise decomposition shows that, in this strategy, the solution is mainly supported by Galileo, with 7 satellites, while the contributions from GLONASS, with 0.18 satellite, and BeiDou, with 0.81 satellite, become residual, and GPS is reduced to approximately 4 satellites. This limitation is directly associated with (i) the total number of satellites transmitting triple-frequency signals in each constellation and (ii) the tracking capabilities of the RBMC receivers, whose firmware restricts the collection of certain signals, significantly reducing the number of satellites available for forming the triple-frequency combination. In the case of GLONASS, a severe decrease is observed in the number of satellites with effective support for three tracked frequencies; for GPS, there is an approximate 40% reduction in the number of satellites usable in this configuration. For BeiDou, the absence or low availability of B2a observations in the analyzed RINEX files limits the use of combinations based on modernized BDS-3 signals, making the solution dependent on the observations effectively tracked and recorded by the receivers, especially those associated with the B1I/B2I/B3I signals. This limitation is consistent with the scenario described by Zajdel et al. (2022), who highlight that not all signals are supported by receivers due to tracking-channel restrictions, configuration limitations, or outdated firmware.

Figure 5 presents the density maps of positioning discrepancies obtained for March 2024, considering the GRAPHIC, IF2, and IF3 methods, with results aggregated for all selected stations and processed days. The organization of the figure allows the temporal behavior of the East, North, and Up components to be compared among the three processing strategies. The vertical lines indicate the mean convergence time of each component, considering the complete set of stations and analyzed days. In cases where the solution did not meet the convergence criterion within the processing session, the maximum session time, corresponding to 180 minutes, was assigned so that these cases were also incorporated into the aggregated statistics.

Figure 5 – Density maps of positioning discrepancies in the Local Geodetic System for March 2024, considering the GRAPHIC, IF2, and IF3 methods. The vertical lines indicate the mean convergence time for each component.

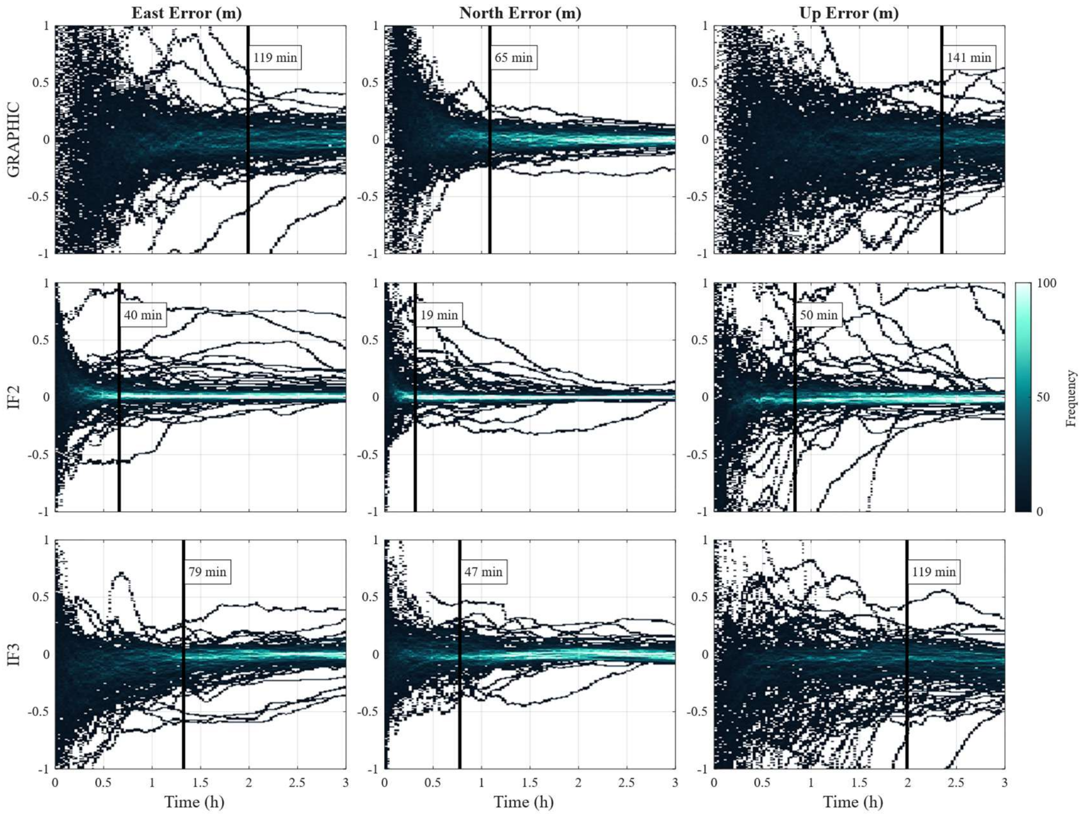

Source: The Authors (2026).

The GRAPHIC method shows greater dispersion throughout the first three hours, with final discrepancies still elevated at some stations. In the final epochs, the mean horizontal errors ranged from approximately 7.2 cm at RSSL to 15.8 cm at BRAZ, while the vertical errors ranged from 8.2 cm at RSSL to 17.9 cm at BRAZ, indicating lower solution stabilization when compared with the ion-free strategies. For the IF2 combination, the best overall performance among the evaluated methods is observed, with a greater concentration of discrepancies close to zero and lower residual error at the end of the processing. In the final epochs, the mean horizontal errors ranged from 1.3 cm at RSSL to 9.0 cm at BRAZ, while the vertical errors ranged from 2.2 cm at RSSL to 8.5 cm at BRAZ. Despite the poorer performance at BRAZ, the IF2 strategy showed a more stable behavior at the other stations, with final errors predominantly at the level of a few centimeters, indicating a better compromise between convergence, stability, and final accuracy. The IF3 strategy showed intermediate performance compared to the other methods, but with more evident degradation in the vertical component. In the final epochs, the mean horizontal errors ranged from 3.1 cm at RSSL to 10.0 cm at BOAV, while the vertical errors ranged from 5.3 cm at RSSL to 17.9 cm at PERC. This behavior indicates that the inclusion of the third frequency did not result, in this experiment, in a systematic improvement of the solution, being especially penalized in the Up component. Compared with IF2, IF3 showed greater residual dispersion and larger formal uncertainties, suggesting that the reduced availability of triple-frequency observations and the consequent geometric degradation limited the potential gains associated with the use of additional signals. Figure 6 presents the density maps of positioning discrepancies obtained for June 2024, considering the methods used, with results aggregated for all selected stations.

Figure 6 – Density maps of positioning discrepancies in the Local Geodetic System for June 2024, considering the GRAPHIC, IF2, and IF3 methods. The vertical lines indicate the mean convergence time for each component.

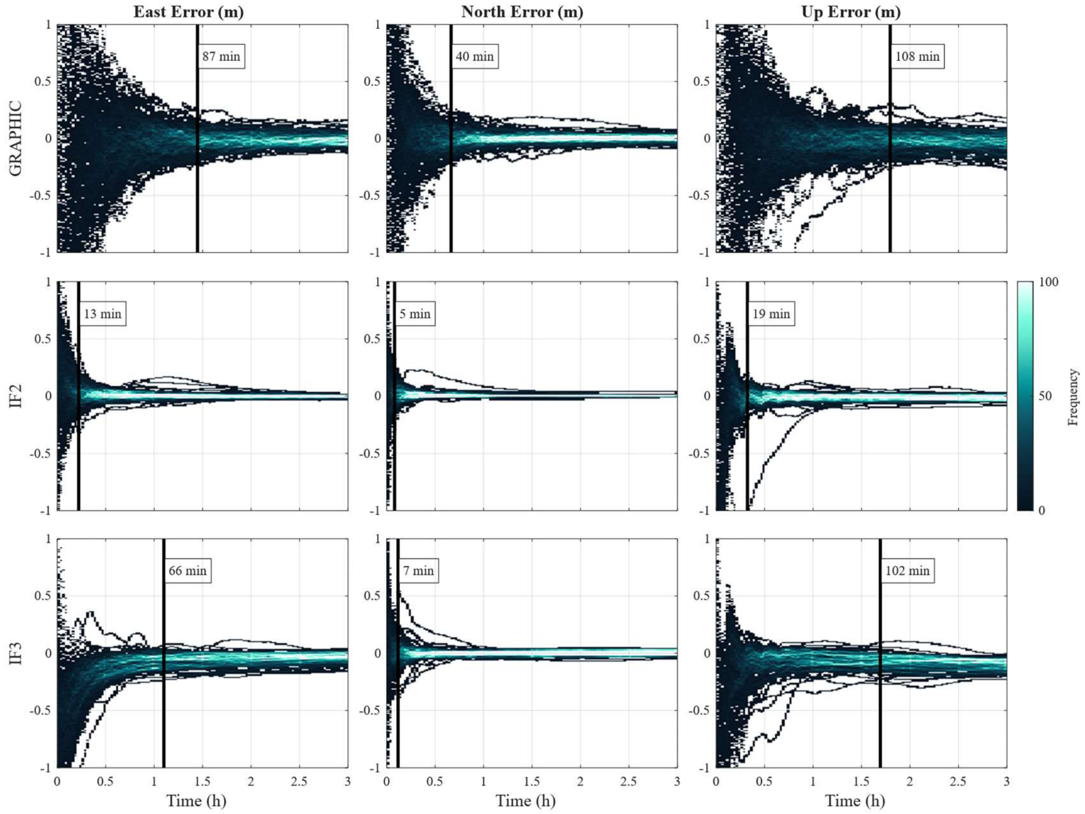

Source: The Authors (2026).

In the final epochs, for GRAPHIC, the mean horizontal errors ranged from approximately 3.4 cm at PPTE to 6.5 cm at RSSL, while the vertical errors ranged from 4.6 cm at PPTE to 7.7 cm at BRAZ, indicating moderate final stabilization, although still inferior to that obtained with IF2. For the IF2 combination, the best overall performance among the evaluated methods is again observed, with a greater concentration of discrepancies close to zero and lower residual error at the end of the processing. In the final epochs, the mean horizontal errors ranged from 0.5 cm at PPTE to 1.2 cm at BOAV, while the vertical errors ranged from 0.9 cm at BOAV to 2.9 cm at PERC. These values indicate predominantly low-centimeter final performance, with small variability among stations and better stabilization of the positional components, especially when compared with GRAPHIC and IF3. The IF3 strategy showed poorer performance than IF2 and, at some stations, also larger residual errors than GRAPHIC, especially in the vertical component. In the final epochs, the mean horizontal errors ranged from approximately 3.2 cm at BRAZ and PERC to 7.9 cm at PPTE, while the vertical errors ranged from 7.6 cm at RSSL to 11.7 cm at BOAV. The vertical penalty was more evident at PERC and BOAV, with final mean errors greater than 11 cm, indicating that the inclusion of the third frequency did not result in a systematic improvement of the solution for this dataset. This behavior suggests that the reduced availability of triple-frequency observations and the possible geometric degradation limited the expected benefits from the use of additional signals.

Considering the results presented in Figures 5, for March, and 6, for June, a clear improvement in the performance of the IF2 combination is observed in relation to the other strategies, both in terms of accuracy and convergence time. In March, IF2 reduced the final horizontal errors by approximately 70 to 85% compared with the GRAPHIC method and by about 50 to 75% compared with the triple-frequency strategy. In the vertical component, these reductions reached 60–80% relative to GRAPHIC and 40–70% relative to IF3. In June, although all methods showed improved performance due to more stable ionospheric conditions, IF2 still maintained an advantage, with typical reductions of 50–70% compared with GRAPHIC and 30–60% compared with the triple-frequency strategy. Regarding convergence time, the results indicate that IF2 converged significantly faster: in March, the reduction was on the order of 30% to 50% compared with the triple-frequency strategy, while in June this difference remained relevant, although smaller, ranging from 20 to 40%. Figure 7 presents the observation residuals as a function of elevation angle for March 2024, considering the GRAPHIC, IF2, and IF3 methods, with results aggregated for all analyzed stations.

Figure 7 – Observation residuals as a function of elevation angle for March 2024, considering the GRAPHIC, IF2, and IF3 methods. The first three rows correspond to pseudorange, and the last three rows correspond to carrier phase observations.

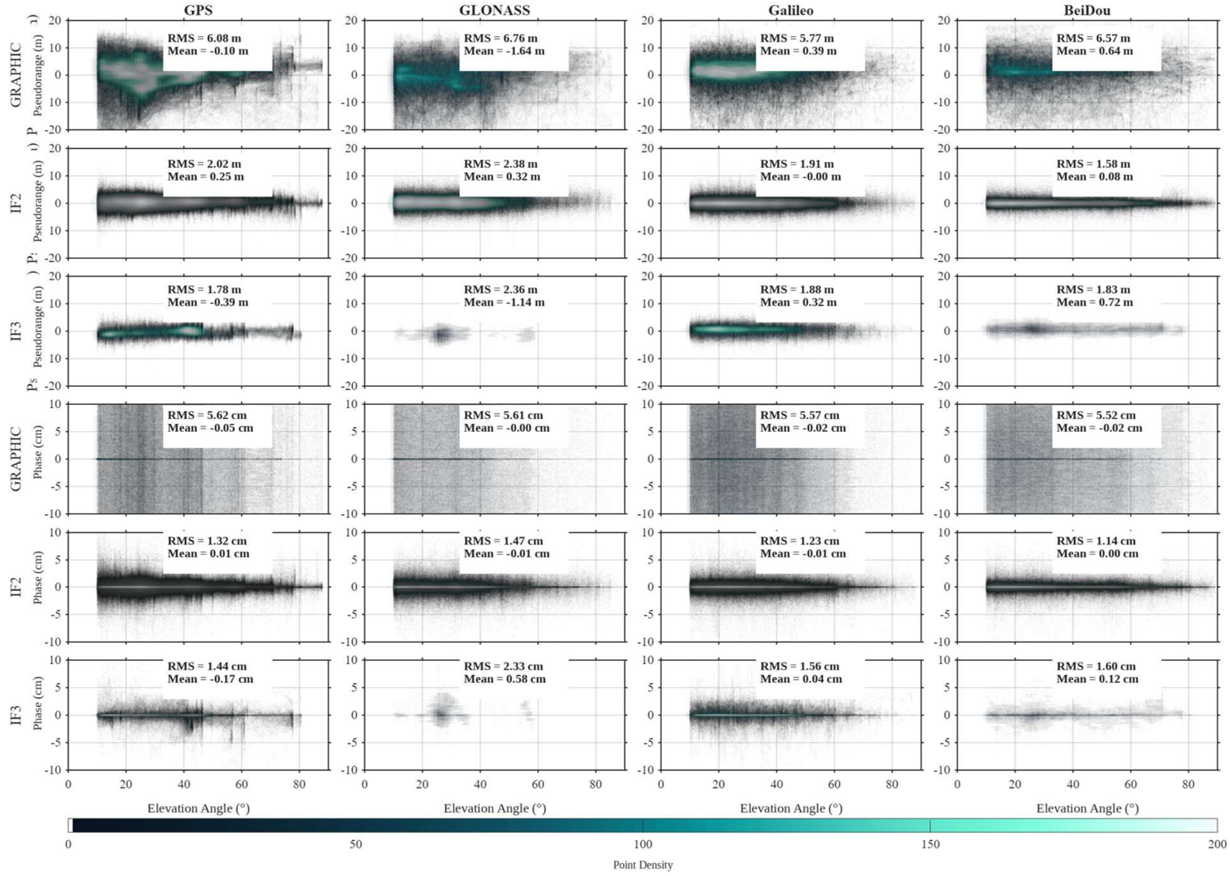

Source: The Authors (2026).

Figure 8 presents the observation residuals, for different methods, as a function of elevation angle for June 2024, with results aggregated for all analyzed stations. The residuals show the expected behavior as a function of elevation, with greater dispersion for satellites close to the horizon and a gradual reduction at higher elevations, due to the shorter atmospheric path and the lower relative influence of multipath and measurement noise. This effect is more evident in the pseudorange observations, whereas the carrier-phase residuals of the ion-free combinations remain more concentrated around zero, with predominantly centimeter-level variations. In the case of GRAPHIC, the use of the quasi-carrier propagates the pseudorange noise, degrading the phase-related residuals when compared with the IF2 and IF3 combinations. The greatest concentration of residuals close to zero generally occurs in intermediate elevation ranges, where there is greater geometric recurrence of the observations and more favorable link conditions. When comparing the analyzed months, June shows slightly lower RMS values and a more controlled distribution, consistent with the lower ionospheric variability of the period. However, the difference relative to March is not necessarily proportional to the scintillation intensity, since the quality control removes discrepant observations and reduces the weight of degraded observations through the inflation of their uncertainties. Thus, the most severe effects of scintillation tend to be more clearly reflected in observation availability, solution stability, and convergence time than only in the final residuals analyzed.

 DOI: http://dx.doi.org/10.14393/rbcv78n0a-81258

Figure 8 – Observation residuals as a function of elevation angle for June 2024, considering the GRAPHIC, IF2, and IF3 methods. The first three rows correspond to pseudorange, and the last three rows correspond to carrier phase observations.

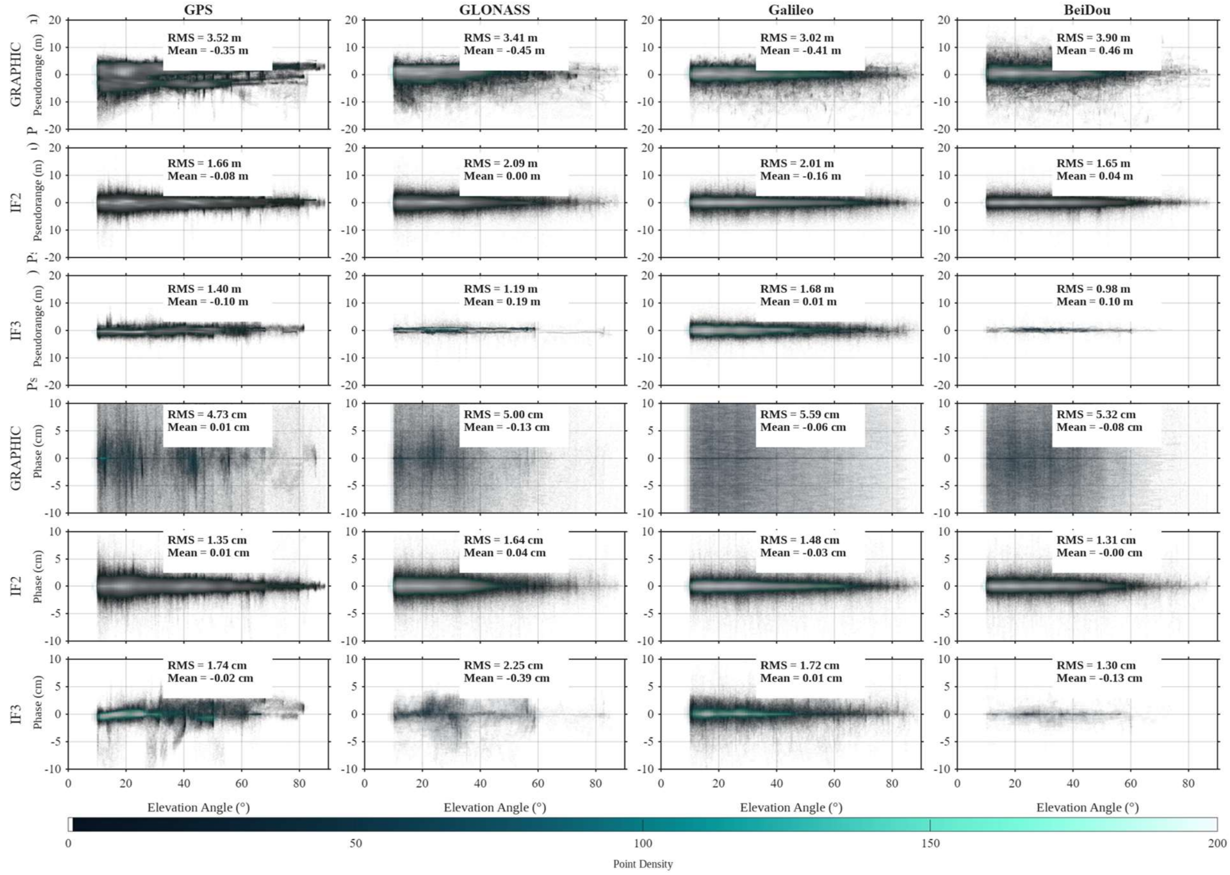

Source: The Authors (2026).

5 CONCLUSION

The analysis conducted in this study made it possible to compare, at Brazilian RBMC stations, the performance of multi-GNSS PPP using three ionospheric mitigation strategies, including the GRAPHIC method and dual- and triple-frequency ion-free combinations, considering periods with contrasting ionospheric variability, namely March and June 2024. Initially, it was observed that observation availability is a structural factor determining the behavior of the solution: the dual-frequency combination preserved an effectively multi-constellation scenario, with a higher mean number of satellites per epoch and more favorable geometry, whereas the triple-frequency combination sharply reduced the set of valid satellites, with loss of constellation diversity and consequent geometric degradation, as evidenced by the increase in PDOP among stations (Figure 4). This limitation, associated with the lower availability of simultaneous tracking on three frequencies, explains a relevant part of the poorer performance observed for the triple-frequency strategy, regardless of the analyzed month.

The results obtained in this study, although still preliminary, partially differ from what is reported in the literature, where triple-frequency solutions usually provide benefits mainly in reducing convergence time and handling residual ionospheric effects, while gains in final accuracy tend to be limited. In the present work, however, the IF3 strategy did not outperform the IF2 combination. This can be explained by factors associated with the adopted strategy and modeling, including the direct use of the triple-frequency combination without explicit treatment of inter-frequency biases (IFBs), the consistency of orbit and clock products based on dual-frequency processing, and the lower effective availability of triple-frequency observations, which negatively affects the solution geometry. In addition, the analysis was conducted under tropical ionospheric conditions, which are more challenging and less explored in controlled studies reported in the literature, potentially amplifying these limitations. Therefore, the results do not invalidate the potential benefits of triple-frequency combinations, but indicate that their practical application critically depends on the adopted modeling strategy, signal availability, and propagation environment considered.

In terms of positioning accuracy, the density maps revealed consistent differences among the evaluated strategies for each month. In March (Figure 5), under higher ionospheric variability, greater temporal and inter-station dispersion was observed for all methods, with cases of persistent degradation throughout the three-hour processing sessions. In this scenario, the dual-frequency ion-free combination generally presented smaller final discrepancies and faster convergence, especially in the horizontal components, while the vertical component remained more sensitive and required a longer time to stabilize. The GRAPHIC method showed greater dispersion and lower stability, whereas the triple-frequency strategy was penalized in both convergence time and final accuracy, with more evident degradation in the vertical component. In June (Figure 6), under more favorable ionospheric conditions, the solutions showed a more controlled behavior, with a greater concentration of discrepancies at centimeter levels and lower dispersion than in March. Even so, the dual-frequency combination maintained the best overall performance, while the triple-frequency combination did not provide systematic improvement, especially in the vertical component. The GRAPHIC method showed greater residual variability associated with the propagation of pseudorange noise into the quasi-carrier observable.

The evaluation of residuals as a function of elevation angle (Figures 7 and 8) reinforced the characteristic behavior of the GNSS link, with greater dispersion at low elevations and a gradual reduction in dispersion as the elevation angle increases. This effect is associated with the longer atmospheric path, greater susceptibility to multipath, and geometric degradation at grazing angles. This pattern was more pronounced in pseudorange observations, while carrier-phase residuals remained concentrated around zero, with predominantly centimeter-level variations. The comparison among methods showed that the dual-frequency combination presented lower dispersion across the entire elevation range, indicating better control of the effective noise, whereas the GRAPHIC method exhibited greater spreading, especially at low elevations. The triple-frequency strategy showed an intermediate behavior, but with greater pseudorange variability than the dual-frequency combination, especially in March. Compared with March, June presented more controlled residuals and lower RMS values in part of the analyses. However, this difference is not as pronounced in the plots, since the analyzed residuals already reflect the processing quality control, with outlier removal and reduced weighting of degraded observations.

In summary, the results indicate that, for the set of stations and conditions evaluated, the dual-frequency strategy provided the best compromise among observation availability, geometry, convergence speed, and final performance. In contrast, the triple-frequency strategy was systematically penalized by the reduction in the number of useful satellites and by geometric degradation, resulting in longer convergence time and larger final residual errors, mainly in the vertical component and during the period of higher ionospheric variability. These findings reinforce that the potential gains associated with the use of additional signals critically depend on the effective multi-constellation availability on three frequencies and on the conditions of the propagation medium. Thus, the operational adoption of the triple-frequency strategy should be accompanied by tracking and quality criteria, as well as geometry assessment, to avoid performance losses in tropical scenarios.

As a perspective for future work, specific experiments are recommended during periods of severe ionospheric disturbance, including events associated with intense geomagnetic storms, such as the May 2024 Mother’s Day Storm. In these scenarios, the effects of ionospheric irregularities, scintillation, and rapid variations in TEC tend to be significantly amplified. Investigating these conditions is essential to assess the robustness of multifrequency strategies under extreme conditions and to verify whether increased spectral redundancy can effectively contribute to mitigating the degrading effects of the propagation medium or, alternatively, accentuate limitations already observed under nominal conditions.

References

Aguiar, C. R., Monico, J. F. G., & Moraes, A. O. (2025). Impact of ionospheric scintillations on GNSS availability and precise positioning. *Space Weather*, 23, e2024SW004217. DOI: 10.1029/2024SW004217.

Ashby, N. (2003). Relativity in the Global Positioning System. *Living Reviews in Relativity*, 6, 1. DOI:

10.12942/lrr-2003-1

Ashby, N. (2004). The Sagnac effect in the Global Positioning System. In G. Rizzi & M. L. Ruggiero (Eds.), *Relativity in rotating frames*: Relativistic physics in rotating reference frames (pp. 11–28). Kluwer Academic Publishers.

Basu, S., Groves, K. M., Basu, S., & Sultan, P. J. (2002). Specification and forecasting of scintillations in communication/navigation links: current status and future plans. Journal of Atmospheric and Solar-Terrestrial Physics, 64(16), 1745–1754. DOI: 10.1016/S1364-6826(02)00124-4

Blewitt, G. (1990). An automated editing algorithm for GPS data. *Geophysical Research Letters*, 17(3), 199–202.

Choy, S. (2009). *An investigation into the accuracy of single frequency precise point positioning (PPP)* [Doctoral dissertation, RMIT University].

Dal Poz, W. R., Silva, A. C., Santos, A. P. dos, Medeiros, N. das G., Ferreira, Í. O., & Oliveira, J. C. de. (2025). Impacts of the Great May 2024 geomagnetic storm on precise point positioning. *Revista Brasileira de Geografia Física,* 18(3), 1697–1713. DOI: 10.26848/rbgf.v18.3.p1697-1713

Deo, M., & El-Mowafy, A. (2017). Triple-frequency GNSS models for PPP with float ambiguity estimation: performance comparison using GPS. *Survey Review*, 50(360), 249–261. DOI: 10.1080/00396265.2016.1263179

Elsheikh, M., Iqbal, U., Noureldin, A., & Korenberg, M. (2023). *The implementation of precise point positioning (PPP): a comprehensive review*. Sensors, 23, 8874. DOI: 10.3390/s23218874

Ge, Y., Dai, P., Qin, W., Yang, X., Zhou, F., Wang, S., & Zhao, X. (2019). Performance of multi-GNSS precise point positioning time and frequency transfer with clock modeling. Remote Sensing, 11, 347. DOI: 10.3390/rs11030347

Glaner, M. F., & Weber, R. (2023). An open-source software package for precise point positioning: raPPPid. *GPS Solutions*, 27, 174. DOI: 10.1007/s10291-023-01488-4

Hauschild, A. (2017). Combinations of observations. In: P. J. G. Teunissen & O. Montenbruck (Eds.), *Springer handbook of global navigation satellite systems*. Springer.

Hobiger, T. & Jakowski, N. (2017). Atmospheric Signal Propagation. In: P. J. G. Teunissen & O. Montenbruck (Eds.), *Springer handbook of global navigation satellite systems*. Springer.

Jiang, X., Li, H., Guo, L., Ye, D., Yang, K., & Li, J. (2024). Research on the Ionospheric Delay of Long-Range Short-Wave Propagation Based on a Regression Analysis. *Remote Sensing*, 16(3), 553. DOI: 10.3390/rs16030553

Klobuchar, J. A. (1987). Ionospheric time-delay algorithm for single-frequency GPS users. *IEEE Transactions on Aerospace and Electronic Systems*, AES-23(3), 325–331.

Kouba, J., Lahaye, F., & Tétreault, P. (2017). Precise Point Positioning. In: Teunissen, P. J. G.; Montenbruck, O. (eds) *Springer Handbook of Global Navigation Satellite Systems*. Springer, Berlin.

Landskron, D., & Böhm, J. (2018). VMF3/GPT3: Refined discrete and empirical troposphere mapping functions. Journal of Geodesy, 92(4), 349–360. DOI: 10.1007/s00190-017-1066-2

Li, M., & Yuan, Y. (2021). Estimation and analysis of the observable-specific code biases estimated using multi-GNSS observations and global ionospheric maps. *Remote Sensing*, 13(16), 3096. DOI: 10.3390/rs13163096

Marques, H. A., Monico, J. F. G., Marques, H. A. S., Susi, M., Borio, D., Park, J., & Węzka, K. (2025). Evaluating GPS and Galileo Precise Point Positioning (PPP) Under Various Ionospheric Conditions During Solar Cycle 25. *Remote Sensing*, 17(18), 3169. DOI: 10.3390/rs17183169

Matsuoka, M. T., Collischonn, C., Klein, I., Camargo, P. O., & Pereira, V. A. S. (2013). Impacto de tempestade geomagnética na ionosfera e no posicionamento com GNSS: estudo de caso para 20 de novembro de 2003 na região brasileira. Boletim de Ciências Geodésicas.

Monico, J. F. G. (2008). *Posicionamento pelo GNSS: descrição, fundamentos e aplicaçõe*s. (2. ed.). Editora

UNESP.

Monico, J. F. G., de Paula, E. R., Moraes, A. O. et al. (2022). The GNSS NavAer INCT project overview and main results. *J. Aerosp. Technol. Manag*., vol. 14. DOI: 10.1590/jatm.v14.1249

Montenbruck, O., Schmid, R., Mercier, F., Steigenberger, P., Noll, C., Fatkulin, R., Kogure, S., & Ganeshan, A. (2015). GNSS satellite geometry and attitude models. *Advances in Space Research*, 56(6), 1015–1029. DOI: 10.1016/j.asr.2015.06.019

Montenbruck, O., Steigenberger, P., Prange, L., Deng, Z., Zhao, Q., Perosanz, F., Romero, I., Noll, C., Stürze, A., Weber, G., Schmid, R., MacLeod, K., & Schaer, S. (2017). The Multi-GNSS Experiment (MGEX) of the International GNSS Service (IGS): Achievements, prospects and challenges. *Advances in Space Research*, 59(7), 1671–1697. DOI: 10.1016/j.asr.2017.01.011

Moraes, A. O., de Paula, E. R., Muella, M. T. A. H., & Perrella, W. J. (2014). On the second order statistics for GPS ionospheric scintillation modeling. *Radio Science*, 49(2), 94–105. DOI: 10.1002/2013RS005270

Schönemann, E. (2014). *Analysis of GNSS raw observations in PPP solutions*. [Doctoral dissertation, Technische Universität Darmstadt].

Shi, C., Gu, S., Lou, Y., & Ge, M. (2012). An improved approach to model ionospheric delays for single-frequency precise point positioning. *Advances in Space Research*, v. 49, n. 12, p. 1698–1708. DOI: 10.1016/j.asr.2012.03.016

Sousasantos, J., Rodrigues, F.S., Moraes, A.O. et al. (2024). On the estimation of scintillation severity using background F-region peak densities: description and example results using GOLD observations. *GPS Solut 28*, 62. DOI: 10.1007/s10291-023-01602-6

Su, K., & Jin, S. (2019). Triple frequency carrier phase precise time and frequency transfer models for BDS 3. *GPS Solution*s, 23, 86. DOI: 10.1007/s10291-019-0879-2

Su, K., Jin, S., & Jiao, G. (2020). Assessment of multi-frequency global navigation satellite system precise point positioning models using GPS, BeiDou, GLONASS, Galileo and QZSS. *Measurement Science and Technology*, 31. DOI: 10.1088/1361-6501/ab69d5

Tegedor, J., & Øvstedal, O. (2014). *Triple carrier precise point positioning (PPP) using GPS L5*. Survey Review, 46(337). DOI: 10.1179/1752270613Y.0000000076

Teunissen, P. J. G., & Montenbruck, O. (Eds.). (2017). *Springer handbook of global navigation satellite systems*. Springer. DOI: 10.1007/978-3-319-42928-1

Tian, Y., Gong, X., Zheng, F. et al. (2026). An instantaneous and reliable precise point positioning integer ambiguity resolution method based on multistage residual tests. *GPS Solut 30*, 6. DOI: 10.1007/s10291-025-01974-x

Veettil, S. V., Aquino, M., Marques, H. A., & Moraes, A. (2020). Mitigation of ionospheric scintillation effects on GNSS precise point positioning (PPP) at low latitudes. *Journal of Geodesy*, 94, 15. DOI: 10.1007/s00190-020-01345-z

Wang, Z., Wang, R., Wang, Y., Hu, C., & Liu, B. (2022). Modelling and assessment of a new triple-frequency IF1213 PPP with BDS/GPS. Remote Sensing, 14(18), 4509. DOI: 10.3390/rs14184509

Wu, J. T., Wu, S. C., Hajj, G. A., Bertiger, W. I., & Lichten, S. M. (1993). Effects of antenna orientation on GPS carrier phase. *Manuscripta Geodaetica*, 18(2), 91–98. DOI: 10.1007/BF03655303

Wu, Z., Wang, Q., Yu, Z., Hu, C., Liu, H., & Han, S. (2022). Modeling and performance assessment of precise point positioning with multi-frequency GNSS signals. *Measurement*. DOI: 10.1016/j.measurement.2022.111687

Xiang, Y., Gao, Y., & Li, Y. (2020). Reducing convergence time of precise point positioning with ionospheric constraints and receiver differential code bias modeling. *Journal of Geodesy*, 94(8). DOI: 10.1007/s00190-019-01334-x

Yang, H., Ren, X., Liu, M., & Zhang, X. (2024). Dual-frequency to five-frequency real-time precise point positioning using new BDS-3 PPP-B2b service. *Earth, Planets and Space*, 76, 82. DOI: 10.1186/s40623-

024-02031-6

Yang, Z., & Morton, Y. T. J. (2025). Impacts of the May 2024 extreme geomagnetic storm on global high-accuracy GPS positioning solutions. *Space Weather*, 23. DOI: 10.1029/2025SW004547

Zajdel, R., Steigenberger, P., & Montenbruck, O. (2022). On the potential contribution of BeiDou-3 to the realization of the terrestrial reference frame scale. *GPS Solutions*, 26, 109. DOI: 10.1007/s10291-022-01298-0

Zaupa, J. P. V., Alves, D. B. M., & Setti Jr, P. T. (2022). Influência da ionosfera no posicionamento por ponto GPS e multi-GNSS em diferentes períodos do dia. [Trabalho apresentado]. XII CBCG (Colóquio Brasileiro de Ciências Geodésicas) e V SBG (Simpósio Brasileiro de Geomática), Curitiba, PR, Brasil.

Zaupa, J. P. V. (2025). *Posicionamento por ponto preciso multi-GNSS: implementação e análises*. [Dissertação de Mestrado, Universidade Estadual Paulista “Júlio de Mesquita Filho”]. Repositório Institucional UNESP. https://hdl.handle.net/11449/313230.

Zaupa, J. P. V., Alves, D. B. M., & Setti Jr, P. T. (2025). Robustez das combinações livres da ionosfera no PPP multi-GNSS sob diferentes níveis de variabilidade ionosférica para uma estação de monitoramento brasileira. I Congresso Internacional de Regularização Fundiária & VIII Simpósio Brasileiro de Ciências Geodésicas e Tecnologias da Geoinformação (I CIRF & VIII SIMGEO), Recife, PE, Brazil. DOI: 10.5281/zenodo.17135729

Zaupa, J. P. V., Alves, D. B. M., & Setti Jr., P. T. (2026a). APPPOLO: A Brazilian processing software for multi-GNSS precise point positioning. *ISPRS Annals of the Photogrammetry, Remote Sensing and Spatial Information Sciences*, X-3/W4-2025, 379–385. DOI: 10.5194/isprs-annals-X-3-W4-2025-379-2026

Zaupa, J. P. V., de Souza, F. T. L., Ferreira, L. G., Yamashiro, H. Y., Gouveia, T. A. F., Alves, D. B. M., Monico, J. F. G., Pereira, V. A. S., & Setti Júnior, P. T. (2026b). Ionospheric and neutrosphere impacts on multi-GNSS kinematic PPP during geomagnetic storms: A global study. *Sensors*, 26(13), 4037. DOI: 10.3390/s26134037

Zhang, Q., Zhao, L., & Zhao, L. (2021). A two-step robust adaptive filtering algorithm for GNSS kinematic precise point positioning. *Chinese Journal of Aeronautics*, 34(10), 210–219. DOI: 10.1016/j.cja.2020.10.033

Acknowledgements

The authors thank the Brazilian Institute of Geography and Statistics (IBGE) for providing data from the Brazilian Network for Continuous Monitoring of GNSS Systems (RBMC), the INCT GNSS-NavAer for providing the ionospheric scintillation data, and the Center for Orbit Determination in Europe (CODE) for the precise products used in the processing. This research was partially funded by the São Paulo Research Foundation (FAPESP), grant no. 2024/22757-0, and by the Brazilian National Council for Scientific and Technological Development (CNPq), grant nos. 306112/2023-0 and 313902/2025-9.

Author Contributions

João P. V. Zaupa: conceptualization, methodology, software, data curation, formal analysis, investigation, validation, visualization, writing – original draft, and writing – review and editing. Daniele B. M. Alves: conceptualization, methodology, supervision, project administration, funding acquisition, resources, and writing – review and editing. Paulo T. Setti Jr.: methodology, validation, formal analysis, supervision, resources, and writing – review and editing.

Conflicts of Interest

The authors declare no conflicts of interest.

 DOI: http://dx.doi.org/10.14393/rbcv78n0a-81258

Biography of the Main Author

João Pedro Voltare Zaupa, born in Álvares Machado, São Paulo, Brazil, is a Ph.D. candidate in Cartographic Sciences at São Paulo State University (UNESP), Presidente Prudente, Brazil. He received his M.Sc. degree in Cartographic Sciences from the same institution, with an emphasis on Geodetic Positioning. His research interests include Precise Point Positioning (PPP), multi-GNSS processing, ambiguity resolution, and ionospheric effects on GNSS signals.

Esta obra está licenciada com uma Licença Creative Commons Atribuição 4.0 Internacional – CC BY. Esta licença permite que outros distribuam, remixem, adaptem e criem a partir do seu trabalho, mesmo para fins comerciais, desde que lhe atribuam o devido crédito pela criação original.